SVU-International Journal of Engineering Sciences and Applications (2023) 4(1): 29-34
Print ISSN 2785-9967 | Online ISSN 2735-4571
DOI 10.21608/svusrc.2022.152944.1062

Stress Analysis of a Rectangular Shaft Carrying a Rotor System Due to Eccentricity

Khalid Elias Hammo [1],

Abstract Rotating machinery is used in several mechanical system affected by exogenous or endogenous vibration due to unbalance, misalignment and cracks, which leads to generate extra forces on shaft and bearings. This research is dedicated to study the unbalance and dissimilarity of shaft on both stresses and deflections of rotor supported by a film of oil bearing. Different rotational speeds (1000 - 4400) rpm and unbalance effects (0.0001-0.0003) m, have been considered. A dynamic model system of the shaft has a rectangular cross – section of (30 x 15) mm^2 and with a mass of 6 kg. The parameters of rotor-shaft, which represented by the value of stiffness coefficients and journal bearing represented by both stiffness and damped coefficients were simulated using MATLAB/ Simulink software, so that, the reaction forces are calculated. Finite Element Program (ANSYS) has been used to analysis of the stresses for the shaft and bearings produced eccentricity and rotation.

Keywords:. Eccentricity, Shaft Dissimilarity, Simulation, Rotor-Shaft system.

1 Introduction

The unbalance of a rotor system is one of the major reasons for the rotating machinery vibration. There are several reasons of unbalancing rotor system, which are represented by defective materials, errors during processing and assembling, dissimilarity of structure, change in temperature during operation, and wearing of a rotor. The unbalance of any rotor occurs due to un coincident of the axis of rotation of the rotor with the geometric axis, and this leads to induce forces due to the inertial rotation.

Several devices have been developed to reduce the stresses-induced vibration, such as Electro-Magnetic Bearings (EMB), lateral force actuators, active balancers … etc. The ideal balance is hard to achieved in experiments, but can be reduced by making the principal axis of inertia coincide with the rotational axis of rotor. [1][2]

A number of researches and analytical methods have been performed to investigate the stress analysis of a rotor-shaft systems, such as finite element technique (ANSYS), (ICM), (MBM), ... etc. Kh. E., Hammo et al [3] focused on the stresses and deflection due to unbalance in flexible circular shaft conducted by film of oil bearing. A finite element simulation of a flexible rotor has been presented in this work. Various values of eccentricities and rotational speed has been taken in consideration. They found that the max. deflection was take place at the midpoint of the shaft while the stresses and deflection are concentrating at the bottom of the bearing due to concentrating forces on this area. Wenjun Yang et al [4] investigate the vibration differential equation of a shaft - disc rotor system by the model synthesis method. Runge-Kutta ‘s direct integration method has been used to extract the equation of system. They found that the effect of shaft-rotor system makes the frequency of rotor to decrease while the various rotation velocities have a small effect on the frequency of the rotor. Also, they found a small effect of eccentricity distance on the stability of the rotor.

Xiaohe Ran et ai [5] are enhance the shaft-rotor system by using two improvement schemes which are rotor stiffness, rotor strength as well as the effect of uni-lateral magnetic extension on the deflected rotor. They used finite element method (ANSYS) to modal, investigate stress and extended unilateral magnetic. The result shows good simulation for the illustration of shaft-rotor system enhanced by predicted schemes and present more excellent stiffness and strength when compared with

Received: 27 July 2022/ Accepted: 12 October 2022
Corresponding Author : Khalid Elias Hammo, khalid1974@uomosul.edu.iq
1. Mechanical Engineering Department, College of Engineering, University of Mosul, Mosul, Iraq

traditional scheme. Lin, Y. and Cheng, L. [6] investigate in them research the complexity of optimal design for flexible rotor support criterion, by using strain energy method. They employed stiffness support and clearance squeeze film dampers (SFDs) and transfer
matrix component mode synthesis method (TMCMS) as design variables
and dynamic analysis of the system respectively. Jian Li, et al [7] studied the influence of dissimilarity for radial clearance at ends of bearings and rotor misalignment on the performance of hydro-dynamic rotor-bearing systems. A technique of finite difference is used to resolve of Reynolds equation and realization of the solution technique is conducted by rapprochement with preceding studies. Mogal, S. P. et al [8] are used the technique of order system for vibration analysis of rotor system to diagnose fault. In order analysis, both phase and amplitude are obtained and the fault type and location are identified. Experimental results show the effect of order analysis to investigate the fault.

Sinha, J. K. et al [9] are invented a process that can dependably appreciate rotor unbalance and mis-alignment from running down of single machine. Zhiwei Huang [10] was established a model which is directly worked based on dual-rotor system equipped with coupling faults of mis-alignment and impact. The model shows an estimation of dynamical system via numerical system, as parallel and angular misalignment varied. The results show significant complexity relative to the frequency at high amplitude with 1/3 X component.

2 Objective of this research

In this research, a flexible shaft with a rectangular cross-sectional area has been performed, mounted on oil film bearing. By using two analytical methods represented by finite element and MATLAB programs, stresses analysis has been investigated. A MATLAB programs has been used to calculate the reaction forces due to rotation. These forces represented by the stiffness of shaft, damping coefficients and ANSYS program to estimate stresses on the shaft during rotation.

3 Mathematical Model and Developed Equation of Motion

The mechanical system is modelled mathematically as a rectangular shaft with a single disc mounted on its mid span. The recent design of rotor-shaft system is shown in figure (1). The geometric centers of bearings, shaft and mass rotor are C_1, C_2 and C_3 respectively. M_R and M_J are the masses of rotor and journal bearings respectively. The dimensions and material properties are tabulated in Table (1).

Table (1): Rotor dimensions and materials properties

Description	Unite (m)	Properties		
		Elastic Modulus (Pa)	Poisson's ratio	Density (kg/m^3)
Rectangular shaft dimensions	0.03 x 0.015	209e9	0.3	7800
Length of the shaft	0.75			
Rotor diameter	0.12			
Rotor thickness	0.01			
Bearing diameter	0.025			
Length of the bearing	0.0125			

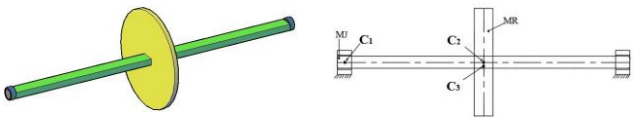

Fig. 1 Rotor-Shaft system model by oil-film bearings.

The nonlinear equation of motion for rotor in both vertical and horizontal directions are [11]:

$$M_R \ddot{Y}_2 + (K_s \cos^2 \omega t + K_w \sin^2 \omega t)(Y_2 - Y_1) + (K_s - K_w)\sin \omega t \cos \omega t (Z_2 - Z_1) = Me\omega^2 \cos(\omega t + \alpha) \quad \ldots\ldots. (1)$$

$$M_R \ddot{Z}_2 + (K_s - K_w)\sin \omega t \cos \omega t (Y_2 - Y_1) + (K_s \sin^2 \omega t + K_w \cos^2 \omega t)(Z_2 - Z_1) \quad \ldots\ldots.. (2)$$

$$= Me\omega^2 \sin(\omega t + \alpha) - Mg$$

$$M_J \ddot{Z}_1 + K_{BYZ} Y_1 + K_{BZZ} Z_1 + C_{BZY} \dot{Y}_1 + C_{BZZ} \dot{Z}_1 = \frac{1}{2}(K_s - K_w)\sin \omega t \cos \omega t (Y_2 - Y_1) \quad \ldots.. (3)$$

$$+ \left(\frac{K_s}{2}\sin^2 \omega t + \frac{K_w}{2}\cos^2 \omega t\right)(Z_2 - Z_1)$$

$$M_J \ddot{Y}_1 + K_{BYY} Y_1 + K_{BYZ} Z_1 + C_{BYY} \dot{Y}_1 + C_{BYZ} \dot{Z}_1$$
$$= \left(\frac{K_s}{2} \cos^2 \omega t + \frac{K_w}{2} \sin^2 \omega t\right)(Y_2 - Y_1) \quad \ldots. (4)$$
$$+ \frac{1}{2}(K_s - K_w) \sin \omega t \cos \omega t (Z_2 - Z_1)$$

Where $Y_1, \dot{Y}_1, \ddot{Y}_1$ *and* $Z_1, \dot{Z}_1, \ddot{Z}_1$ the position, velocity and rate of velocity or acceleration of the bearings in Y and Z directions respectively, while $Y_2, \dot{Y}_2, \ddot{Y}_2$ *and* $Z_2, \dot{Z}_2, \ddot{Z}_2$ for the rotor in the same direction. K_s *and* K_w are the shaft stiffness in both directions.

$K_{BYY}, K_{BYZ}, K_{BZY}, K_{BZZ}$ *and* $C_{BYY}, C_{BYZ}, C_{BZY}, C_{BZZ}$ are stiffness, damping properties of the bearings, figure (2). Me_w^2 and **Mg** represent unbalance and gravity forces. e is the eccentricity; and ω is the angular velocity of rotation.

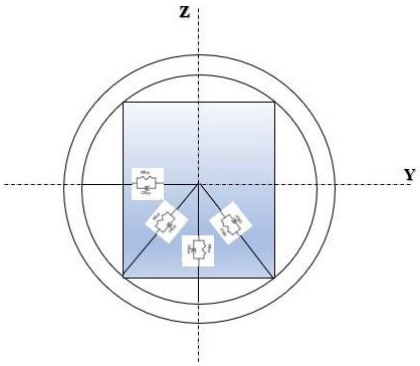

Fig. 2 The model of Journal bearing.

4 Results and discussion

Simulation results for a rectangular shaft of a single rotor with three values of the eccentricity (e = $0.1x10^{-3}$ to $0.3x10^{-3}$) were presented to study these effects with many various rotational speeds (N = 1000 to 4400 rpm) on the number of stresses and deflections on the shaft. Elastic and shear moduli as well as Poisson's ratio of the adopted material were numerically represented in Table (1). Using uniformly distributed load of 5 N, tensile stresses and deflections were obtained for all cases. Many types of stresses and deflections in all directions for this shaft are obtained and discussed as following:

In figures (3, 4,5,6) when the eccentricity (e = $0.1x10^{-3}$) the value of Von Mises stress (σ_{von}) begins from (33) Mpa at (N= 1000 R.P.M) and reach to (36.5) Mpa at (N= 4400 R.P.M) but (under the same conditions) in the case of the eccentricity (e = $0.3x10^{-3}$) will be (43) Mpa at (N= 1000 R.P.M) and reach to (161) Mpa at (N= 4400 R.P.M). In figures (7,8,9,10), when the eccentricity (e = $0.1x10^{-3}$) the value of (σ_3) stress begin from (-39.4) Mpa at (N= 1000 R.P.M) and reach to (-41.7) Pa at (N= 4400 R.P.M) but (under the same conditions) in the case the eccentricity (e = $0.3x10^{-3}$) will be (-51.1) Mpa at (N= 1000 R.P.M) and reach to (-203) Mpa at (N= 4400 R.P.M). In figures (11,12,13,14) when eccentricity (e = $0.1x10^{-3}$) the value of deflection in the X-axis U_x begin from (-4.9 µm) at (N= 1000 R.P.M) and reach to (-114 µm) at (N= 4400 R.P.M) but (under the same conditions) in the case of the eccentricity (e = $0.3x10^{-3}$) will be(-15.8 µm) at (N= 1000 R.P.M) and reach to (-346 µm) at (N= 4400 R.P.M). Figure (15) shows the variation of (σ_{von}) versus (N) is negligible at lowering speeds and it then increases at higher speeds (in same path) from (33) to (43) pa in the case of eccentricity (e = $0.1x10^{-3}$) and from (31.3) to (98.5) Mpa for (e = $0.2x10^{-3}$) and from (36.5) to (161) Mpa for (e = $0.3x10^{-3}$) with increase of (N) from 1000 to 4400 R.P.M but it is reach a max. values which are (84.3), (135) and (187) Mpa respectively at (N= 4200 R.P.M). At higher speeds, the variation of (U_y) with respect to (N) is negligible and it increases at higher speeds (in same path) from (-85.8) to (25.6) µm in the case of eccentricity (e = $0.1x10^{-3}$) and from (-79.7) to (142) µm for (e = $0.2x10^{-3}$) and from (-109) to (258) µm for (e = $0.3x10^{-3}$) with increase of (N) from 1000 to 4400 R.P.M. but it is reach a max. Values which are (-188), (-283) and (-380) µm respectively at (N= 4200 R.P.M). At the end of simulation, the values of all stresses and deflections of the shaft carrying rotor are listed in table (2).

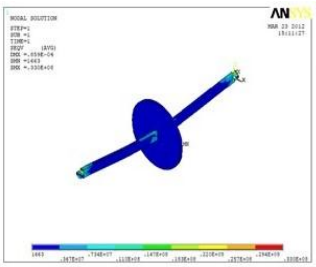

Fig. 3 Contour of the stress distribution of (σ_{von}) stress on the shaft at (e = $0.1x10^{-3}$ & N = 1000 R.P.M).

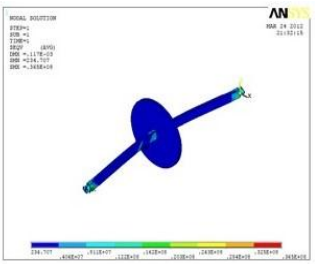

Fig. 4 Contour of the stress distribution of (σ_{von}) stress on the shaft at (e = $0.1x10^{-3}$ & N = 4400R.P.M).

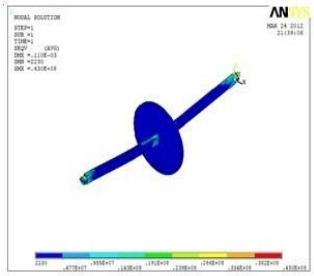

Fig. 5 Contour of the stress distribution of (σ_{von}) stress on the shaft at (e = 0.3 & N = 1000R.P.M).

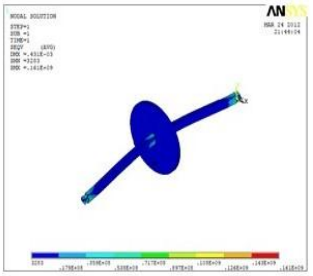

Fig. 6 Contour of the stress distribution of (σ_{von}) stress on the shaft at (e = 0.3 & N = 4400R.P.M).

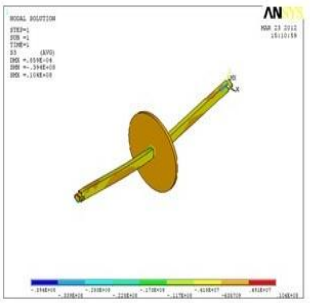

Fig. 7 Contour of the stress distribution of (σ_3) stress on the shaft at (e = 0.1 & N = 1000R.P.M).

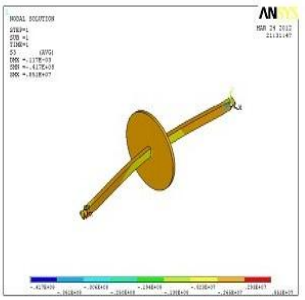

Fig. 8 Contour of the stress distribution of (σ_3) stress on the shaft at (e = 0.1 & N = 4400R.P.M).

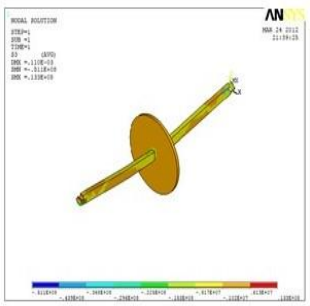

Fig.9 Contour of the stress distribution of (σ3) stress on the shaft at (e = 0.3 & N = 1000R.P.M).

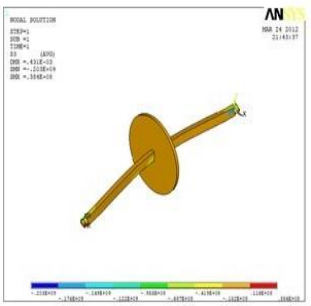

Fig. 10 Contour of the stress distribution of (σ_3) stress on the shaft at (e = 0.3 & N = 4400R.P.M).

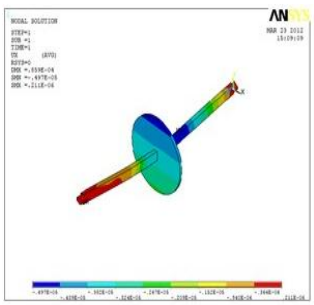

Fig. 11 Deflection distribution (U_x) in the shaft at (e = 0.1 & N = 1000R.P.M).

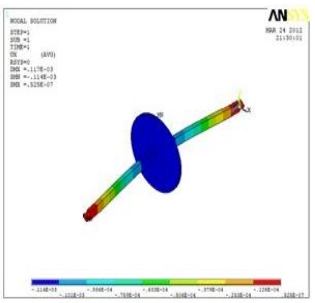

Fig. 12 Deflection distribution (U_x) in the shaft at (e = 0.1 & N = 4400 R.P.M).

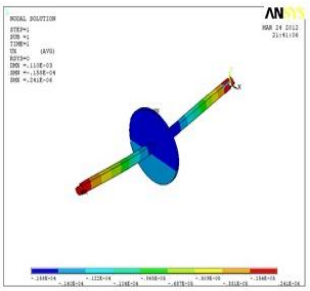

Fig. 13 Deflection distribution (U_x) in the shaft at (e = 0.3 & N = 1000 R.P.M).

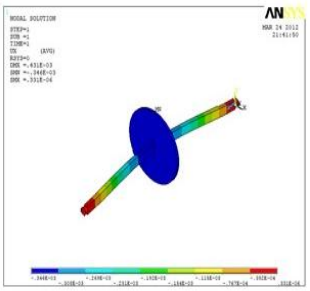

Fig. 14 Deflection distribution (U_x) in the shaft at (e = 0.3 & N = 4400 R.P.M).

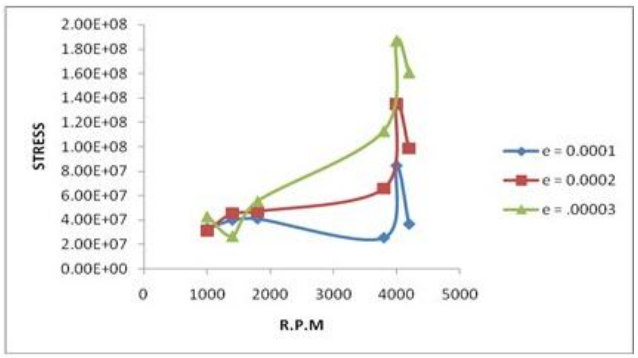

Fig. 15 Effect of Rotational Speed (R.P.M) on σ_{von} in the rotor for three different values of eccentricity.

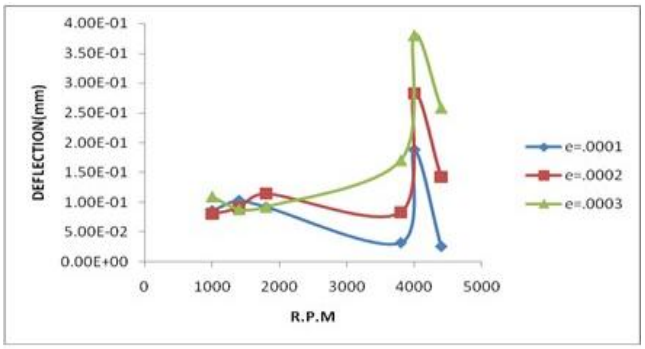

Fig. 16 Effect of Rotational Speed (R.P.M) on U_Y in the rotor for three different values of eccentricity.

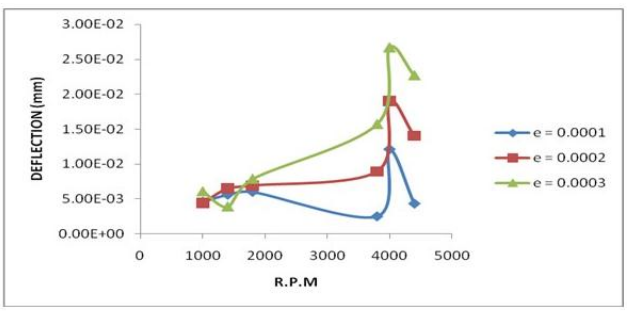

Fig. 17 Effect of Rotational Speed (R.P.M) on U_Z in the rotor for three different values of eccentricity.

Table (2): Results of all cases of the values of eccentricity and rotational speed.

Stresses & Deflections	Ecc. = $0.1*10^{-3}$		Ecc. = $0.2*10^{-3}$		Ecc. = $0.3*10^{-3}$	
	1000 rpm	4400 rpm	1000 rpm	4400 rpm	1000 rpm	4400 rpm
$\sigma_1\ (MPa)$	41.9	42.8	39.6	123.0	54.4	203
$\sigma_3\ (MPa)$	-39.4	-41.7	-37.2	-124	-51	-203
$\sigma_{Von}\ (MPa)$	33	36.5	31.3	98.5	43	161
$U_x\ (\mu m)$	-4.9	-114	-11	-231	-15.8	-346
$U_y\ (\mu m)$	-85.8	25.6	-79.7	142	-109	258
$U_z\ (\mu m)$	4.55	-4.63	11.2	241	6.05	22.7
$U_{sum}\ (\mu m)$	85.9	117	80.3	277	110	431

5 Conclusion

A simulation of rotor bearing system has been presented in this work by using a finite elements technique and MATLAB software. The effects of eccentricity and shaft dissimilarity are investigated. From figures of stresses and deflections, it can be noticed that there is sharp rising in the curves when the speed is (N= 4000 R.P.M), and this mean that the system frequency reaches to its natural frequency (i.e., in the vicinity of resonance phenomena). We can also notice that the maximum deflection is take place in the larger face of the shaft (0.75 x 0.03 m^2) because of increasing elasticity in this face and it's clearly shown in figure (16) and this leads to occur a maximum stress. It can be designing a rotating shaft in this form with considering of reduce the value of eccentricity.

References

1. Liqing Li et al, "Review of Rotor Balancing Methods", Machines, Vol.9, No. 89, 2021. https://doi.org/10.3390/machines9050089.
2. Andrés B. O. et al, "Active vibration control of a rotor-bearing system based on dynamic stiffness", Rev. Fac. Ing. Univ. Antioquia N.° 55. September 2010.
3. Hammo Kh. E. et al, "The Effect of Unbalance on the Cyclic Stresses of a Flexible Rotor Mounted on Oil-Film Bearings Using Finite Elements Technique (ANSYS)", Al-Rafidain Engineering Vol.22 No. 1 February 2014.
4. Wenjun Yang et al, "Dynamic Analysis of Flexible Shaft and Elastic Disk Rotor System Based on the Effect of Alford Force", Shock and Vibration, Volume 2019, Article ID 3545939, 13 pages https://doi.org/10.1155/2019/3545939.
5. Xiaohe Ran et al, "Dynamic Analysis and Mechanical Structure Improvement of Submersible Rotor", IEEE, Vol. 7, 2019.
6. Lin, Y. and Cheng, L., "Optimal Design of Complex Flexible Rotor-Support Systems using Minimum Strain Energy under Multi-Constraint Conditions", Journal of Sound and Vibration (1998), 215(5), 1121-1134.
7. Jian Li et al, "Influence of dissimilar radial clearances on the performance of hydro dynamic rotor-bearing systems considering misalignment effects", Journal of Engineering Tribology, 2018, Vol. 232(3), 231-243.
8. Mogal, S. P. et al, "Experimental investigation of unbalance and misalignment in rotor bearing system using order analysis", Journal of Measurements in Engineering, December 2015, Vol. 3, Issue 4, 114-122.
9. Sinha, J. K. et al, "Estimating unbalance and misalignment of a flexible rotating machine from a single run-down", Journal of Sound and Vibration 272 (2004) 967–989.
10. Zhiwei Huang, "Dynamic characteristics of dual-rotor system with coupling faults of

misalignment and rub-impact", MATEC Web of Conferences 139, 00122 (2017), DOI: 10.1051/matecconf/201713900122.

11. Imam I et al, "Development of an On-Line Rotor Crack Detection and Monitoring", Journal of Vibration, Acoustics, Stress, and Reliability in Design July 1989, Vol. 111/241.

Appendix

```
>> clear
L=0.75;
b=0.03;
h=0.015;
t=0.01;
D=0.12;% Dia. of Rotor
r=0.025;% Dia of Bearing
E=209*10^9;
V1=(b*h*L);
V2=(pi*D^2*t);
d=7800;
M=V1*d+V2*d;
Mj=1.5;
N=1000;
w=2*pi*N/60;
n=0.4;
KYY=(4*(pi^2*(2-n^2)+16*n^2))/(pi^2*(1-n^2)+(16*n^2))^(3/2);
KZZ=(4*(pi^2*((12-n^2)*(1+2*n^2))+(32*n^2*(1-n^2))))/((1-n^2)*(pi^2*(1-n^2)+16*n^2)^(3/2));
KYZ=(pi*(pi^2*(1-n^2)^2-16*n^4))/(n*((1-n^2)^(1/2))*(pi^2*(1-n^2)+16*n^2)^(3/2));
KZY=-1*(pi*(pi^2*(1-n^2)*(1+2*n^2)+(32*n^2*(1+n^2))))/(n*((1-n^2)^(1/2)*(pi^2*(1-n^2)+16*n^2)^(3/2)));
CYY=(2*pi*(1-n^2)^(1/2)*(pi^2*(1+2*n^2)-16*n^2))/(n*(pi^2*(1-n^2)+16*n^2)^(3/2));
CZZ=(2*pi*(n^2*(1-n^2)^2+48*n^2))/(n*((1-n^2)^(1/2))*(pi^2*(1-n^2)+16*n^2)^(3/2));
CYZ=-1*(8*(pi^2*(1+2*n^2)-16*n^2))/((pi^2*(1-n^2)+(16*n^2))^(3/2));
CZY=CYZ;
c1=0.0005;
P=9.81*(M/2+Mj);
KBYY=((KYY*P)/c1)*0+2.8e6;
KBZZ=((KZZ*P)/c1)*0+4.05e6;
KBYZ=((KYZ*P)/c1)*0;
KBZY=((KZY*P)/c1)*0;
CBYY=((CYY*P)/(c1*w));
CBZZ=((CZZ*P)/(c1*w));
CBYZ=((CYZ*P)/(c1*w));
CBZY=CBYZ;
I1=b*h^3/12;
I2=b^3*h/12;
I3=pi*(D)^4/64;
L1=L/2-t/2;
KY=-48*E*I3/(-L^3+8*L1^3*(1-I3/I1));
KZ=-48*E*I3/(-L^3+8*L1^3*(1-I3/I2));
e=0.0001;
```